

Entanglement entropy scaling transition under competing monitoring protocols

Mathias Van Regemortel,* Ze-Pei Cian, Alireza Seif, Hossein Dehghani, and Mohammad Hafezi
*Joint Quantum Institute, College Park, 20742 MD, USA and
The Institute for Research in Electronics and Applied Physics,
University of Maryland, College Park, 20742 MD, USA*

(Dated: March 13, 2022)

Dissipation generally leads to the decoherence of a quantum state. In contrast, numerous recent proposals have illustrated that dissipation can also be tailored to stabilize many-body entangled quantum states. While the focus of these works has been primarily on engineering the non-equilibrium steady state, we investigate the build-up of entanglement in the quantum trajectories. Specifically, we analyze the competition between two different dissipation channels arising from two incompatible continuous monitoring protocols. The first protocol locks the phase of neighboring sites upon registering a quantum jump, thereby generating a long-range entanglement through the system, while the second one destroys the coherence via dephasing mechanism. By studying the unraveling of stochastic quantum trajectories associated with the continuous monitoring protocols, we present a transition for the scaling of the averaged trajectory entanglement entropies, from critical scaling to area-law behavior. Our work provides novel insights into the occurrence of a measurement-induced phase transition within a continuous monitoring protocol.

Entanglement of a quantum mechanical system has been a mystifying property ever since the beginning days of quantum mechanics. With notable examples, such as the Einstein-Podolski-Rosen paradox or the Bell inequalities, the notion of entanglement has truly acquired a status of embracing the fundamental counter-intuitive nature of quantum mechanics [1]. While the coupling of a quantum system with the environment is often detrimental for preserving entanglement, dissipation can also be engineered and utilized to stabilize exotic, highly entangled many-body states [2, 3]. With the development of recent experimental platform, such as circuit quantum electrodynamics (QED) [4–7] and Rydberg polaritons [8], it is now possible to generate strongly entangled photonic states by reservoir engineering [9] and tailoring schemes of dissipation [10–15].

Quantum phase transitions [16] typically come with different phases for the ground state entanglement entropy, as was shown for the exemplary Bose-Hubbard model [17] after numerous works investigated the scaling of correlations [18–20]. Also local projective measurements of a quantum state destroy the entanglement generated by unitary evolution, which may lead to a phase transition of entanglement entropy across the system. In this context, a number of works have recently explored quantum circuits consisting of random unitaries alternated with local measurements, and a phase transition was seen for the scaling of entanglement entropy [21–24]. Later a similar transition was reported for the stochastic trajectories from quantum systems under a local continuous-monitoring protocol, which induces an interplay with the entanglement generated by the unitary dynamics of the system Hamiltonian [25–27]. More generally, it is interesting to investigate whether stochastic quantum trajectories, a well-established quantum optics formalism [28, 29], can provide more insight into

measure-induced phase transitions.

In this Letter, we present a scaling transition of entanglement entropy in a quantum system that is entirely governed by dissipative dynamics – coming from the interplay of two continuous monitoring protocols – in the *absence* of unitary dynamics. In Fig. 1(a), we illustrate the model; a chain of bosonic modes, of length L and with open boundaries, is first monitored with a protocol that locks the phase of two adjacent sites, characterized by the jump operators

$$d_j \equiv (a_j^\dagger + a_{j+1}^\dagger)(a_j - a_{j+1}), \quad (1)$$

where a_j (a_j^\dagger) is the annihilation (creation) operator for the bosonic mode on site j [2]. The second monitoring protocol is dephasing, associated with the jump operators

$$c_j \equiv a_j^\dagger a_j. \quad (2)$$

The rates of the monitoring for phase-locking (d_j) and dephasing (c_j) are given by Λ and Γ , respectively. We investigate the competition between these two monitoring schemes in terms of the ratio of monitoring rates, or the *reduced* dephasing rate

$$\gamma \equiv \frac{\Gamma}{\Lambda}. \quad (3)$$

The aspect of continuous monitoring and the recording of the corresponding jumps is a crucial element of this work. Therefore, while dissipation is often introduced to account for the decoherence of a quantum state, we elaborate specific implementation schemes that allow for the continuous tracking of the system in a circuit QED setup. The random occurrence and detection of the quantum jumps (1) and (2) implies that the dynamics of a quantum state $|\psi(t)\rangle$ is inherently stochastic, as depicted in Fig. 1(b). To characterize the state of the system, we use

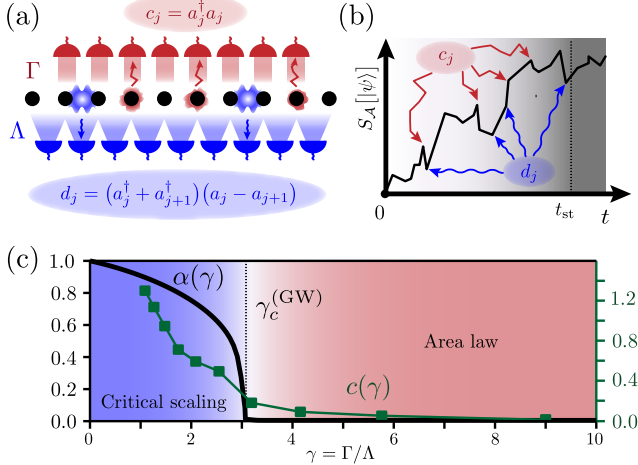


Figure 1. A schematic illustration of our setup and the main results. (a) We analyze the stochastic evolution of the system under continuous monitoring with two competing monitoring protocols, as represented by the jump operators d_j and c_j with the rates Λ and Γ , respectively. (b) The quantum state $|\psi(t)\rangle$, starting from zero entropy, is expected to follow a stochastic trajectory under the continuous monitoring with d_j and c_j , which can be seen as random fluctuation of entanglement entropy of a subsystem in the chain. Over long enough times t_{st} , the system is expected to converge to a steady state which can be sampled over. (c) The main result: A comparison of the order parameter α that we find in the Gutzwiller approach and the effective central charge $c(\gamma)$, with $\gamma \equiv \Gamma/\Lambda$, as obtained by a fitting procedure with the functional form of critical scaling from Eq. (8) in system with $L = 32$.

the associated entanglement entropy of the state $|\psi(t)\rangle$ of a subsystem \mathcal{A} , a *state-dependent* quantity, which is evaluated as $S_{\mathcal{A}}[|\psi(t)\rangle] = -\text{Tr}\rho_{\mathcal{A}} \log \rho_{\mathcal{A}}$ with $\rho_{\mathcal{A}}$ the reduced density matrix of the state $|\psi(t)\rangle$ on \mathcal{A} . It is of fundamental importance that $S_{\mathcal{A}}$ is a strongly *nonlinear* function of the stochastic states $|\psi(t)\rangle$. As an immediate consequence, statistical averages of $S_{\mathcal{A}}[|\psi(t)\rangle]$ over the states can *not* be retrieved from a master equation approach, in stark contrast with linear quantities such as, most notably, operator expectation values $\langle O \rangle_t = \langle \psi(t) | O | \psi(t) \rangle$ [28, 30]. Importantly, there is a convergence time t_{st} for $S_{\mathcal{A}}$, after which the stochastic state $|\psi(t)\rangle$ is sampled from a steady-state distribution.

The key result is a scaling transition seen in the statistically averaged entanglement entropy of stochastic states after some evolution time, as presented in Fig. 1(c): we find a change of the scaling of entanglement entropy across a critical value of the reduced dephasing rate 3. When phase-locking dominates, the state is a superfluid and entanglement entropy has a critical scaling with subsystem size, characterized by an effective central charge $c(\gamma)$ (green line). When dephasing takes over, the behavior changes to an area law, marked by $c(\gamma) \approx 0$. Remarkably, we can formulate an intuitive Gutzwiller mean-field

approach for the system in the thermodynamic limit and introduce an order parameter α (black line), which shows a sharp transition and vanishes at a critical value $\gamma_c^{(\text{GW})}$, close to the critical value found numerically for the scaling of trajectory entanglement entropy. A similar transition was seen in a number of recent works that investigated the competition between Hamiltonian dynamics and the stochastic dynamics from dephasing monitoring, both for hard-core bosons [25] and free fermions [26, 27]. In a circuit, two incompatible types of measurements, *without* unitary entangling gates, can also lead to a scaling transition for entanglement entropy of the stochastic states [31, 32]. With our work, we aim to extend the recent understanding of a measurement-induced phase transition, as seen in discrete random circuits, to the stochastic trajectories of an unraveling that is associated with the continuous monitoring of a quantum system.

Stochastic trajectories.— The system dynamics is solely governed by the two competing monitoring protocols and has no unitary dynamics from a Hamiltonian. A state $|\psi(t)\rangle$ then follows a stochastic trajectory, as was originally introduced in the seminal works [28, 30] as a way to stochastically sample the master equation of the density matrix ρ in an open quantum system. Whereas the *unraveling* of a master equation in terms of stochastic trajectories that average to the system density matrix $\rho(t)$ is not unique, in this work, on the contrary, it relates unequivocally to the specific monitoring protocol that we present, as pictured in Fig. 1(a)-(b), thereby relying explicitly on the hypothesis of detector-dependent stochastic pure-state dynamics [29].

The sampling of quantum trajectories from the continuous monitoring goes as follows. At time t , we evaluate whether there is a jump in the differential time interval $[t, t + \Delta t]$ by evaluating the probability

$$\begin{aligned} \Delta p &= \Delta t \left(\Lambda \sum_{j=1}^{L-1} \langle \psi(t) | d_j^\dagger d_j | \psi(t) \rangle + \Gamma \sum_{j=1}^L \langle \psi(t) | c_j^\dagger c_j | \psi(t) \rangle \right) \\ &= \sum_{j=1}^{L-1} \Delta p_j^{(d)} + \sum_{j=1}^L \Delta p_j^{(c)}, \end{aligned} \quad (4)$$

which is a summation over the probabilities $\Delta p_j^{(d)}$ and $\Delta p_j^{(c)}$ of the jumps d_j and c_j to occur, respectively.

We then draw a random number $0 < r < 1$. If $\Delta p < r$, no jump is detected in our monitoring scheme and we evolve the state over Δt with the anti-Hermitian Hamiltonian $H_{\text{eff}} = -\frac{i\Lambda}{2} \sum_{j=1}^{L-1} d_j^\dagger d_j - \frac{i\Gamma}{2} \sum_{j=1}^L c_j^\dagger c_j$. If $\Delta p > r$ a jump f is recorded, which we select from the jumps d_j (1) and c_j (2) with probabilities $\Delta p_j^{(d)}$ and $\Delta p_j^{(c)}$, respectively, to evaluate $|\psi(t + \Delta t)\rangle = f|\psi(t)\rangle$.

After each time step Δt , the state $|\psi(t)\rangle$ is renormalized and then we simulate the stochastic evolution of $|\psi_i(t)\rangle$ in the monitoring scheme. It is important to realize that the detection of a quantum jump (with prob-

ability Δp) as well as the *absence* of a jump (probability $1 - \Delta p$) in time interval Δt yields information about the actual state of the system for an observer that tracks the dynamics by monitoring the system. This was recently illustrated in a number of experiments to monitor the stochastic evolution of a superconducting qubit [33–36] and how simultaneously monitoring qubit dephasing and relaxation leads to an interplay [37].

We emphasize that, while the local $U(1)$ symmetry is broken by the phase locking dissipator (1), a global $U(1)$ symmetry is present in our system, stemming from conservation of the total particle number; both jumps d_j (1) and c_j (2) conserve the total particle number. For the upcoming analysis we fix the filling factor n always to $n = 1$ and the evolution of our system starts from the Fock state $|\psi(t=0)\rangle = |\dots1111\dots\rangle$.

Within the presented monitoring scheme, the phase-locking monitoring (1) stabilizes in the long-time limit a pure Bose-Einstein Condensate (BEC) dark state with long-range coherence, where the L particles in the chain are injected in the zero-momentum mode; $|D\rangle = (a_{k=0}^\dagger)^L |0\rangle$, with a_k^\dagger the creation operator of a photon with momentum k . [2, 3]. The dephasing monitoring (2), on the contrary, directs the system to a product state of local Fock states, which has zero entanglement.

Gutzwiller approach.— Given a stochastic trajectory state $|\psi(t)\rangle$, upon taking the the thermodynamic limit $L \rightarrow \infty$, we can study the dynamics of local (i.e. on-site) observables in the Gutzwiller approximation by considering only a mean-field coupling to neighboring sites for the single-site reduced density matrix. An effective single-site Liouvillian can be constructed for the Gutzwiller master equation of the reduced density matrix after averaging over trajectories [38, 39]. We refer the interested reader to the Supplemental Material.

The time evolution of local observables can be evaluated from the Gutzwiller master equation. Before presenting the numerical results, we study the dynamics of the mean-field *order parameter* $\alpha \equiv \langle a \rangle$, and find

$$\partial_t \alpha = 2\Lambda(\langle a^\dagger a^2 \rangle - \langle a^2 \rangle \alpha^*) - \frac{\Gamma}{2} \alpha, \quad (5)$$

where we can readily identify the dark states in two limiting cases. First, when $\Gamma = 0$, there is only phase locking and the steady state is given by $a|\alpha\rangle = \alpha|a\rangle$, which is the case for a coherent state for all the sites. Second, if $\Lambda = 0$, then the pure dephasing dynamics lead to $\alpha \rightarrow 0$ in the long-time limit, i.e., non-diagonal order disappears.

The result of numerical analysis of the order parameter α is shown in Fig. 1(c), where the order parameter vanishes at a critical value $\gamma_c^{(\text{GW})} \approx 3$.

Trajectory entanglement entropy.— We focus on evaluating the Von Neumann entanglement entropy of the trajectory states from a system with size L , $|\psi_L\rangle$, in a

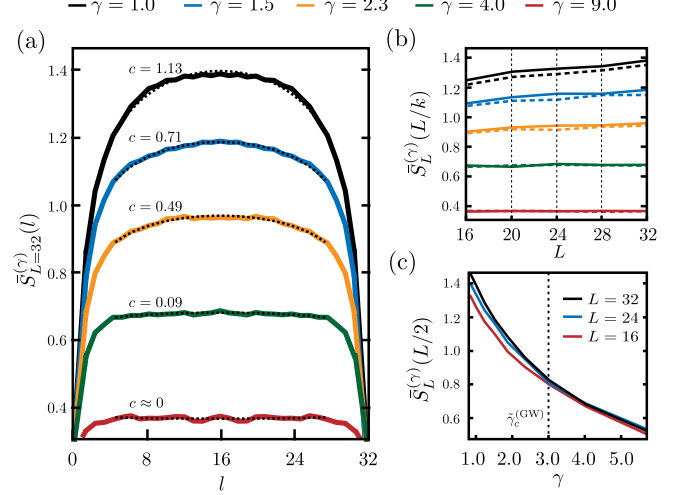


Figure 2. Different scalings of $\bar{S}_L^{(\gamma)}(l)$ from averaging over 10000 trajectory states sampled after reaching the steady state. (a) The scaling of $\bar{S}_{L=32}^{(\gamma)}(l)$ as function of l for different values of the monitoring ratio γ . A transition is seen from critical scaling (black, blue, orange lines) to an area law (green and red line), as obtained from the effective central charges $c(\gamma)$ found by fitting (dotted lines) the functional form (8) (b) The scaling of $\bar{S}_L^{(\gamma)}(L/2)$ (solid) and $\bar{S}_L^{(\gamma)}(L/4)$ (dashed) as function of L . (c) The dependence of $\bar{S}_L^{(\gamma)}(L/2)$ on γ for different system sizes L ; we distinguish a critical point γ_c where the lines start to coincide, close to the Gutzwiller critical point $\gamma_c \approx 3$.

subsystem containing l sites,

$$S(l)[|\psi_L\rangle] = -\text{Tr}[\rho_{\mathcal{A}} \log \rho_{\mathcal{A}}], \quad (6)$$

with $\rho_{\mathcal{A}} = \text{Tr}_{\mathcal{B}}|\psi_L\rangle\langle\psi_L|$, the reduced density matrix of subsystem \mathcal{A} with $l \leq L$ sites, starting from the left boundary, and \mathcal{B} the subsystem with the remaining $L - l$ sites.

We evaluate the averaged trajectory entanglement entropy (6) after obtaining a set of M stochastic trajectory states $|\psi_L^{(\gamma)}(t)\rangle_i$, $i \in [1, M]$, at time t in a system with reduced dephasing rate γ (3),

$$\bar{S}_L^{(\gamma)}(l, t) = \frac{1}{M} \sum_{i=1}^M S(l)[|\psi_L^{(\gamma)}(t)\rangle_i]. \quad (7)$$

Numerical results.— We use Matrix Product States (MPS) [40] to sample the stochastic quantum states [41], thereby making use of the C++ package *ITensor* [42].

In Fig. 2, the scaling of the averaged entanglement entropy $\bar{S}_L^{(\gamma)}(l)$ for trajectories sampled from the steady state is illustrated for the three parameters l (a), L (b) and γ (c). In Fig. 2(a) we see that the curves $\bar{S}_L^{(\gamma)}(l)$ show a transition from a strong concave behavior as function of l when the phase-locking monitoring dominates (black, blue and orange line) to a regime with an area-law behavior (green and red line). After numerical analysis,

we identify the scaling of the curves in the phase-locking regime as logarithmic, reminiscent of the scaling of entanglement entropy for ground states of critical Hamiltonians with open boundary conditions [17], as given by a result from conformal field theory [43],

$$\bar{S}_L^{(\gamma)}(l) = \frac{c(\gamma)}{6} \log \left[\frac{2L}{\pi} \sin \left(\frac{\pi l}{L} \right) \right] + s_0(\gamma). \quad (8)$$

Here $c(\gamma)$ is the effective central charge and $s_0(\gamma)$ the residual entropy. The same scaling was recently found for free fermions subject to dephasing [27].

We perform a fitting procedure (dotted lines) with the functional form (8) to obtain the parameters $c(\gamma)$ (indicated above the curve) and $s_0(\gamma)$ and find a close agreement with the numerical results (solid lines). In Fig. 1(c) we summarize our key result: the comparison between the values found for the effective central charge $c(\gamma)$ from Eq. (8) for a system with $L = 32$, and the mean-field result for the order parameter α from Eq. (5). At the critical reduced dephasing rate $\gamma_c^{(\text{GW})}$ where the order parameter vanishes, we also see a strong suppression of the central charge $c(\gamma)$. Increasing γ further leads to $c(\gamma) \approx 0$; an area law, showing a plateau value for the bulk entanglement entropy given by the residual entropy $s_0(\gamma)$. In the limit $\gamma \rightarrow \infty$ we know that no entanglement can build up and that $\bar{S}_L^{(\gamma)}(l) \rightarrow 0$ so that also $s_0(\gamma) \rightarrow 0$.

The exact critical value γ for the transition of the scaling of $\bar{S}_L^{(\gamma)}(l)$ is difficult to extract from our numerical data. This is mainly because we are computationally limited to sampling relatively small system sizes of $L \lesssim 32$, making it difficult to perform a proper finite-size scaling analysis, as was carried out for the ground-state of the Bose-Hubbard model [17].

Nevertheless, a remarkable agreement is seen on Fig 1(c) between the phase transition for the Gutzwiller order parameter α , inherently in the thermodynamic limit $L \rightarrow \infty$, and the transition for the effective central charge $c(\gamma)$ for a finite system with $L = 32$. While this may seem counterintuitive in light of the non-uniqueness of an unraveling for sampling a master equation, we attribute the agreement to the specific choice of unraveling that we use; by construction of the monitoring protocol, we explicitly establish the unraveling in terms of the quantum jumps (1) and (2). Since all jumps act locally on the system, this unraveling is appropriate for an approximation in terms of the Gutzwiller ansatz for the averaged single-site reduced density matrix of trajectory states, as explained in more detail in the Supplemental Material.

Alternatively, the scaling of entanglement entropy with system size L can be studied, as is shown in Fig 2(b) for the averaged half-chain entanglement entropy $\bar{S}_L^{(\gamma)}(L/2)$ (solid lines) and quarter-chain entanglement entropy $\bar{S}_L^{(\gamma)}(L/4)$ (dashed lines). When γ is below the critical point (black, blue and orange line), a monotonous growing of the entanglement entropy is observed when L is in-

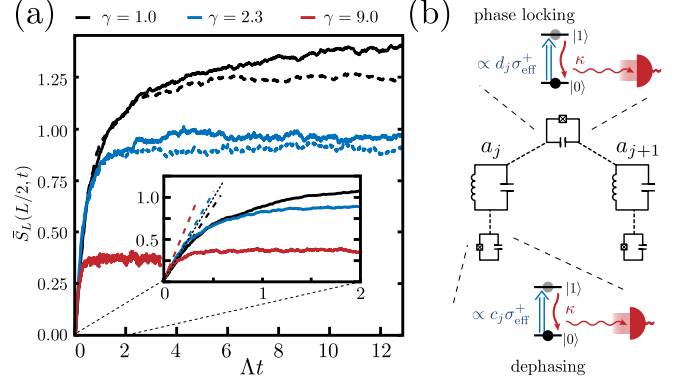


Figure 3. The time evolution of $\bar{S}_L^{(\gamma)}(\frac{L}{2}, t)$ in time for $L = 32$ (solid) and $L = 16$ (dashed) obtained from averaging over 500 trajectories. Below the critical point (black and blue lines) entanglement entropy for different L converge to different values, while above (red lines) it converges to the same steady value. In the inset we show the short-time behavior and see that the initial growth is linear (dashed lines), with a rate close to $\frac{\Delta}{2}$ (dotted line). (b) A schematic of the setup that we propose for the experimental implementation. The cavities are coupled 2-by-2 to dissipative ancilla spins for the phase locking jumps and each cavity is coupled to another ancilla for the dephasing. Registering spontaneous spin decays in the ancillae allows for the registering of cavity jumps.

creased and a significant difference can be distinguished between the curves of half-chain and quarter-chain entanglement entropy, relating back to the critical scaling of the lines seen in Fig. 2(a). In the other regime, when γ is above the critical point and dephasing dominates (green and red lines) both half-chain and quarter-chain entropy coincide and, moreover, remain constant as a function of system size, thus reflecting the area law with a plateau of the residual entropy $s_0(\gamma)$ when $c(\gamma) \approx 0$ in (8), as seen in Fig. 2(a).

Finally, we show in Fig. 2(c) the steady-state scaling of half-chain entropy $\bar{S}_L^{(\gamma)}(L/2)$ as function of γ for different system sizes L to see how the behavior changes across the critical point γ_c . When γ is below γ_c the curves for different L fall apart. Upon increasing γ , $\bar{S}_L^{(\gamma)}(L/2)$ decreases for the different L and when a critical point is reached, close to $\gamma_c^{(\text{GW})} = 3$ found in the Gutzwiller analysis, the curves for different L converge. If γ is increased further beyond the critical point, the curves coincide, thus confirming that $\bar{S}_L^{(\gamma)}(L/2)$ is uniform for different system sizes L in the regime dominated by dephasing, in accordance with the flatness of the green and red curves observed in Fig. 2(b).

To study how entanglement entropy develops over time, we show in Fig. 3 the time evolution of half-chain entanglement entropy $\bar{S}_L^{(\gamma)}(L/2, t)$ for $L = 32$ (solid lines) and $L = 16$ (dashed lines) for different values of γ . The initial state is a product state and has $s_l[|\psi(t=0)\rangle = 0$ for all l . We then let the state evolve

for different γ and sample different Monte Carlo trajectories to see the rise in entanglement entropy across the chain. As shown in the main figure, we can determine a saturation time t_{st} , where $\bar{S}_L^{(\gamma)}(L/2, t)$ converges to a steady-state value, as was schematically depicted in Fig. 1(b). The saturation time t_{st} depends strongly on both the system size L and reduced dephasing rate γ . If we zoom in on short times, shown in the inset of Fig. 3, we see that the initial growth is close to linear (dashed lines), i.e. $\bar{S}_L^{(\gamma)}(L/2, t) = \kappa t$, with $\kappa \approx \frac{\Lambda}{2}$ (dotted line). The evolution of trajectory entanglement entropy is thus reminiscent of the entanglement growth after a quench, where also a linear behavior is seen at short times, which then saturates to a steady value in the long-time limit. [44].

When dephasing is dominant (red lines) we see a rapid convergence of $\bar{S}_L^{(\gamma)}(L/2, t)$ to the steady-state value and the curves for different L are indistinguishable from each other, as expected for the area law. In the regime where phase-locking dominates (blue and black lines) the convergence is much slower, since entanglement now needs to spread between distant sites. We see that systems with different size L (solid vs. dotted lines) now converge to different steady-state values, reflecting the critical scaling of $\bar{S}_L^{(\gamma)}(l)$ on system size L , as previously illustrated more accurately in Fig. 2(b) for the steady-state sampling.

Circuit QED implementation.— As pictured in Fig. 3(b), the two monitoring schemes can be engineered by coupling the cavities to very dissipative ancilla qubits, in which the cavity jumps can be registered as spontaneously emitted photons following an excitation. For the phase-locking d_j , the key idea is to engineer an effective coupling between the two adjacent cavities j and $j + 1$ and the ancilla of the form

$$H_{\text{eff}} \approx g_{\text{eff}} d_j \sigma_j^x, \quad (9)$$

with $\sigma^x = \sigma^+ + \sigma^-$.

Originally the phase-locking dissipation (1) was presented in a cold-atom context [2], but it can also be engineered in circuit QED [45]. In the Supplemental Material, we elaborate in detail a scheme to engineer H_{eff} (9) by coupling the cavities 2-by-2 to a driven ancilla with an anharmonic level structure, such as a fluxonium qubit. [46].

While dephasing noise (2) is ubiquitous in quantum systems and generally leads to heating [47–51], we propose a controlled scheme of dephasing by coupling each cavity to a lossy ancilla qubit with $\sim a^\dagger a \sigma_x$. Upon registering an ancilla decay, one can infer the occurrence of a dephasing jump c_j , as we show in the Supplemental Material. This is in contrast with a recent work, where a cavity-qubit coupling of the form $H \sim a^\dagger a \sigma_z$ was used to monitor the parity of the cavity by performing qubit measurements to detect cavity photon decay [35]. This

is fundamentally from our proposal, where the coupled ancilla serves both to engineer *and* to register the occurrence of the dephasing jump c_j .

Conclusions and outlook.— We have investigated the scaling transition for entanglement entropy averaged over trajectory states $\bar{S}^{(\gamma)}(l)$ in a system with two competing continuous monitoring protocols. A critical value for the reduced monitoring rate γ_c is found where we see a transition from critical entanglement scaling (8) to a regime with an area law for the steady-state trajectory entanglement entropy, as illustrated in Fig. 2. By fitting expression (8) to the curves $\bar{S}^{(\gamma)}(l)$ we obtained an estimate for the critical value γ_c where the central charge vanishes, in close agreement with the critical value found in a Gutzwiller approach for the order parameter α , presented as our main result in Fig. 1(c). At short times, the growth of trajectory entanglement entropy is linear, while it saturates to a steady plateau value at late times, as shown in Fig. 3.

The unraveling of a master equation is not unique and entanglement can depend on the unravelling chosen, which is determined by how the system is monitored [52]. It would be fascinating to investigate if a similar transition can be seen for different unravelings within the same master equation. While trajectory entanglement entropy is a quantity that is most likely challenging (if not impossible) to measure in experiment – it would require several identical copies of the same stochastic state [53, 54] – it would be intriguing to see if exotic quantum states can be stabilized with a feedback protocol that relies on registered jumps within a continuous monitoring protocol [55].

We acknowledge stimulating discussions with Rosario Fazio during the initial formation of this project and subsequent fruitful insights by Oles Shtanko, Luis Pedro Garcia-Pintos, Alexey Gorshkov, Mohammad Maghrebi, Dolf Huybrechts and Michiel Wouters. MVR gratefully acknowledges support in the form of a BAEF postdoctoral fellowship. ZC, AS, HD, and MH were supported by AFOSR FA9550-19-1-0399, ARO W911NF2010232, W911NF-15-1-0397 and NSF Physics Frontier Center at the Joint Quantum Institute. We used the Bridges system, which is supported by NSF award number ACI-1445606, at the Pittsburgh Supercomputing Center (PSC) [56, 57]. The authors acknowledge the University of Maryland supercomputing resources (<http://www.it.umd.edu/hpcc>) made available in conducting the research reported in this paper.

* mvanrege@umd.edu

[1] J. S. Bell, Physics Physique Fizika **1**, 195 (1964).
[2] S. Diehl, A. Micheli, A. Kantian, B. Kraus, H. Büchler, and P. Zoller, Nature Physics **4**, 878 (2008).
[3] B. Kraus, H. P. Büchler, S. Diehl, A. Kantian, A. Micheli,

and P. Zoller, *Physical Review A* **78**, 042307 (2008).

[4] A. Blais, J. Gambetta, A. Wallraff, D. I. Schuster, S. M. Girvin, M. H. Devoret, and R. J. , *Physical Review A* **75**, 032329 (2007).

[5] R. Schoelkopf and S. Girvin, *Nature* **451**, 664 (2008).

[6] A. A. Houck, H. E. Türeci, and J. Koch, *Nature Physics* **8**, 292 (2012).

[7] M. Kounalakis, C. Dicke, A. Bruno, N. K. Langford, and G. A. Steele, *npj Quantum Information* **4**, 1 (2018).

[8] M. Saffman, T. G. Walker, and K. Mølmer, *Reviews of modern physics* **82**, 2313 (2010).

[9] J. Poyatos, J. I. Cirac, and P. Zoller, *Physical review letters* **77**, 4728 (1996).

[10] H. Weimer, M. Müller, I. Lesanovsky, P. Zoller, and H. P. Büchler, *Nature Physics* **6**, 382 (2010).

[11] M. J. Kastoryano, F. Reiter, and A. S. Sørensen, *Physical review letters* **106**, 090502 (2011).

[12] J. Cho, S. Bose, and M. Kim, *Physical review letters* **106**, 020504 (2011).

[13] J. T. Barreiro, M. Müller, P. Schindler, D. Nigg, T. Monz, M. Chwalla, M. Hennrich, C. F. Roos, P. Zoller, and R. Blatt, *Nature* **470**, 486 (2011).

[14] F. Reiter, L. Tornberg, G. Johansson, and A. S. Sørensen, *Physical Review A* **88**, 032317 (2013).

[15] Z.-P. Cian, G. Zhu, S.-K. Chu, A. Seif, W. DeGottardi, L. Jiang, and M. Hafezi, *Physical review letters* **123**, 063602 (2019).

[16] S. Sachdev, *Handbook of Magnetism and Advanced Magnetic Materials* (2007).

[17] A. M. Läuchli and C. Kollath, *Journal of Statistical Mechanics: Theory and Experiment* **2008**, P05018 (2008).

[18] M. P. Fisher, P. B. Weichman, G. Grinstein, and D. S. Fisher, *Physical Review B* **40**, 546 (1989).

[19] T. D. Kühner and H. Monien, *Physical Review B* **58**, R14741 (1998).

[20] S. Ejima, H. Fehske, and F. Gebhard, *EPL (Europhysics Letters)* **93**, 30002 (2011).

[21] M. J. Gullans and D. A. Huse, *arXiv preprint arXiv:1910.00020* (2019).

[22] B. Skinner, J. Ruhman, and A. Nahum, *Physical Review X* **9**, 031009 (2019).

[23] C.-M. Jian, Y.-Z. You, R. Vasseur, and A. W. Ludwig, *Physical Review B* **101**, 104302 (2020).

[24] O. Shtanko, Y. A. Kharkov, L. P. García-Pintos, and A. V. Gorshkov, *arXiv preprint arXiv:2004.06736* (2020).

[25] Y. Fuji and Y. Ashida, *arXiv preprint arXiv:2004.11957* (2020).

[26] X. Cao, A. Tilloy, and A. De Luca, *arXiv preprint arXiv:1804.04638* (2018).

[27] O. Alberton, M. Buchhold, and S. Diehl, *arXiv preprint arXiv:2005.09722* (2020).

[28] J. Dalibard, Y. Castin, and K. Mølmer, *Physical review letters* **68**, 580 (1992).

[29] H. M. Wiseman and J. M. Gambetta, *Physical review letters* **108**, 220402 (2012).

[30] R. Dum, A. Parkins, P. Zoller, and C. Gardiner, *Physical Review A* **46**, 4382 (1992).

[31] A. Lavasani, Y. Alavirad, and M. Barkeshli, *arXiv preprint arXiv:2004.07243* (2020).

[32] M. Ippoliti, M. J. Gullans, S. Gopalakrishnan, D. A. Huse, and V. Khemani, *arXiv preprint arXiv:2004.09560* (2020).

[33] K. Murch, S. Weber, C. Macklin, and I. Siddiqi, *Nature* **502**, 211 (2013).

[34] S. Weber, A. Chantasri, J. Dressel, A. N. Jordan, K. Murch, and I. Siddiqi, *Nature* **511**, 570 (2014).

[35] L. Sun, A. Petrenko, Z. Leghtas, B. Vlastakis, G. Kirchmair, K. Sliwa, A. Narla, M. Hatridge, S. Shankar, J. Blumoff, *et al.*, *Nature* **511**, 444 (2014).

[36] Z. K. Minev, S. O. Mundhada, S. Shankar, P. Reinhold, R. Gutiérrez-Jáuregui, R. J. , M. Mirrahimi, H. J. Carmichael, and M. H. Devoret, *Nature* **570**, 200 (2019).

[37] Q. Ficheux, S. Jezouin, Z. Leghtas, and B. Huard, *Nature communications* **9**, 1 (2018).

[38] J. Lebreuilly, C. Aron, and C. Mora, *Physical review letters* **122**, 120402 (2019).

[39] W. Casteels and M. Wouters, *Physical Review A* **95**, 043833 (2017).

[40] D. Perez-Garcia, F. Verstraete, M. M. Wolf, and J. I. Cirac, *arXiv preprint quant-ph/0608197* (2006).

[41] A. J. Daley, *Advances in Physics* **63**, 77 (2014).

[42] ITensor Library (version 2.0.11) <http://itensor.org>.

[43] P. Calabrese and J. Cardy, *Journal of Statistical Mechanics: Theory and Experiment* **2004**, P06002 (2004).

[44] P. Calabrese and J. Cardy, *Journal of Statistical Mechanics: Theory and Experiment* **2005**, P04010 (2005).

[45] D. Marcos, A. Tomadin, S. Diehl, and P. Rabl, *New Journal of Physics* **14**, 055005 (2012).

[46] S. Girvin, M. Devoret, and R. , *Physica Scripta* **2009**, 014012 (2009).

[47] M. Boissonneault, J. M. Gambetta, and A. Blais, *Physical Review A* **79**, 013819 (2009).

[48] A. Sears, A. Petrenko, G. Catelani, L. Sun, H. Paik, G. Kirchmair, L. Frunzio, L. Glazman, S. Girvin, and R. Schoelkopf, *Physical Review B* **86**, 180504 (2012).

[49] J. Schachenmayer, L. Pollet, M. Troyer, and A. J. Daley, *Physical Review A* **89**, 011601 (2014).

[50] Y. Yanay and E. J. Mueller, *Physical Review A* **90**, 023611 (2014).

[51] J.-S. Bernier, R. Tan, C. Guo, C. Kollath, and D. Poletti, *arXiv preprint arXiv:2003.13809* (2020).

[52] H. Nha and H. Carmichael, *Physical review letters* **93**, 120408 (2004).

[53] A. Elben, B. Vermersch, C. F. Roos, and P. Zoller, *Physical Review A* **99**, 052323 (2019).

[54] H. Pichler, G. Zhu, A. Seif, P. Zoller, and M. Hafezi, *Physical Review X* **6**, 041033 (2016).

[55] H. M. Wiseman, *Physical Review A* **49**, 2133 (1994).

[56] J. Towns, T. Cockerill, M. Dahan, I. Foster, K. Gaither, A. Grimshaw, V. Hazlewood, S. Lathrop, D. Lifka, G. D. Peterson, R. Roskies, J. Scott, and N. Wilkins-Diehr, *Computing in Science & Engineering* **16**, 62 (2014).

[57] N. A. Nystrom, M. J. Levine, R. Z. Roskies, and J. R. Scott, in *Proceedings of the 2015 XSEDE Conference: Scientific Advancements Enabled by Enhanced Cyberinfrastructure*, XSEDE '15 (ACM, New York, NY, USA, 2015) pp. 30:1–30:8.

Supplemental Material

I. THE CIRCUIT IMPLEMENTATION

In this section, we elaborate the experimental implementation of our model within an integrated superconducting circuit. Each cavity is weakly coupled to two ancilla systems, one associated with phase-locking and the other with dephasing monitoring (Eq. (1) and (2), respectively, from main text, illustrated in Fig. 3b). The central idea is that the corresponding jumps can be recorded as spontaneous emission events in the ancillary systems.

We first elaborate in detail the realization of the phase-locking and dephasing jumps and then a simulation of the dephasing and phase-locking scheme is provided.

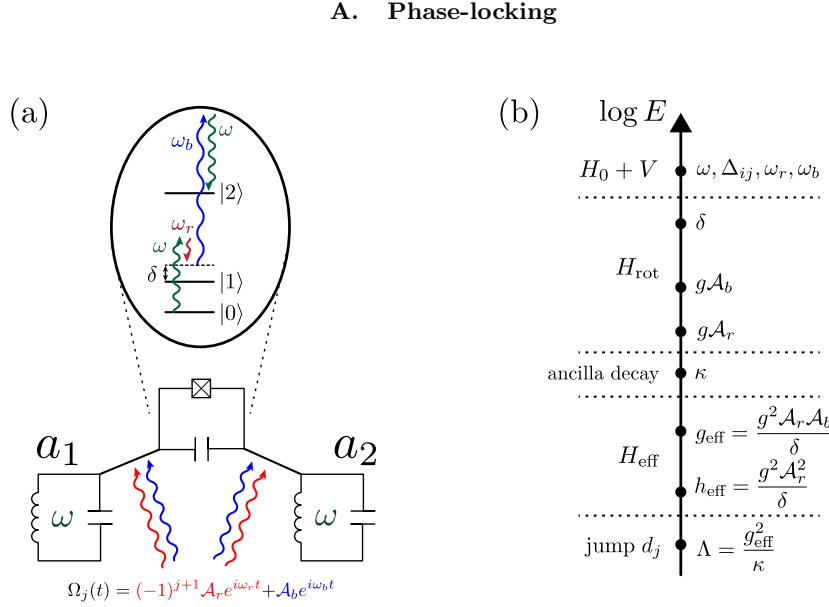


Figure 1. (a) A schematic of the experimental implementation of the phase-locking jump between two cavities with modes a_1 and a_2 . The full setup is irradiated with the two-tone beam $\Omega_j(t)$ to induce the transitions as given in the level diagram for the ancilla. (b) An overview of the hierarchy of energy scales necessary to get from $H_0 + V$, via a rotating wave approximation (H_{rot}), adiabatic elimination (H_{eff}) and a Born-Markov approximation, to the phase-locking jump operators d_j .

We first illustrate the experimental scheme for monitoring the phase-locking jumps $d_j = (a_j^\dagger + a_{j+1}^\dagger)(a_j - a_{j+1})$ for two cavities a_1 and a_2 coupled to an ancilla and will generalize the idea to a full chain at the end. A schematic illustration of the two-cavity setup can be found in Fig. 1(a). Recently, a closely related scheme was also elaborated for engineering two-photon dissipation to stabilize a photon pair condensate [?].

Both cavities are coupled to a strongly anharmonic three-level system, which can be implemented on a circuit with fluxonium or transmon qubits [?]. The coupled Hamiltonian is of the form $H = H_0 + V$, with the free Hamiltonian

$$H_0 = \omega a_1^\dagger a_1 + \omega a_2^\dagger a_2 + \sum_{i=0}^2 \epsilon_i |i\rangle\langle i|, \quad (1)$$

where ϵ_i is the energy of the anharmonic oscillator at the i th level, and the coupling between the cavities and the anharmonic ancilla is induced by a CW drive

$$V = \sum_{j=1}^2 g(a_j + a_j^\dagger)(\Sigma + \Sigma^\dagger)(\Omega_j(t) + \Omega_j^*(t)), \quad (2)$$

where $\Sigma = |0\rangle\langle 1| + \sqrt{2}|1\rangle\langle 2|$ is the annihilation of the anharmonic oscillator and $\Omega_j(t)$, consisting of two tones, one is blue-detuned and the other red-detuned

$$\Omega_j(t) = (-1)^{j+1} \mathcal{A}_r e^{i\omega_r t} + \mathcal{A}_b e^{i\omega_b t}, \quad (3)$$

with $\omega_r = \omega - \Delta_{10} - \delta$ and $\omega_b = -\omega - \Delta_{21} + \delta$ and the ancilla energy level differences $\Delta_{ij} = \epsilon_i - \epsilon_j$. It is important that the amplitude \mathcal{A}_r is antisymmetric, while \mathcal{A}_b is symmetric.

Applying the rotating wave approximation in (2), we find to leading order

$$H_{\text{rot}} = g\mathcal{A}_r(a_1 - a_2)|1\rangle\langle 0|e^{-i\delta t} + g\mathcal{A}_b(a_1^\dagger + a_2^\dagger)|2\rangle\langle 1|e^{i\delta t} + h.c. \quad (4)$$

When the detuning δ is much larger than $|g\mathcal{A}_r|$ and $|g\mathcal{A}_b|$ (weak-coupling regime), the state $|1\rangle$ can be adiabatically eliminated. For this we use Heisenberg equation of motion to find

$$i\partial_t(|1\rangle\langle 0|) = [|1\rangle\langle 0|, H_{\text{rot}}] = ig e^{i\delta t} \left(A_b(a_1^\dagger + a_2^\dagger)|2\rangle\langle 0| - A_r(a_1^\dagger - a_2^\dagger)(|1\rangle\langle 1| - |0\rangle\langle 0|) \right) \quad (5)$$

$$i\partial_t(|2\rangle\langle 1|) = [|2\rangle\langle 1|, H_{\text{rot}}] = ig e^{-i\delta t} \left(-A_r(a_1 - a_2)|2\rangle\langle 0| + A_r(a_1 + a_2)(|2\rangle\langle 2| - |1\rangle\langle 1|) \right). \quad (6)$$

If there is a strong decay κ in the ancilla system (as we quantify below) it will almost always be found in the ground state $|0\rangle$ and the level occupations of $|1\rangle$ and $|2\rangle$ can be neglected, so that $\langle P_0 \rangle \approx 1$ and $\langle P_1 \rangle \approx \langle P_2 \rangle \approx 0$, with the projection operator on ancilla levels $P_n = |n\rangle\langle n|$.

The formal solutions are then found as

$$|1\rangle\langle 0|(t) = ig \int_0^t ds \left(A_b(a_1^\dagger + a_2^\dagger)|2\rangle\langle 0| + A_r(a_1^\dagger - a_2^\dagger) \right) e^{i\delta s}, \quad |2\rangle\langle 1|(t) = -ig A_r \int_0^t ds (a_1 - a_2)|2\rangle\langle 0|e^{-i\delta s} \quad (7)$$

Substituting these solutions in H_{rot} (4) and assuming that δ is much larger than any frequency associated with the cavity-ancilla dynamics, we can make two approximations: (i) we send the integration boundary $t \rightarrow \infty$ (ii) we time-average over the fast oscillations with frequency δ .

After evaluation, we obtain a new effective Hamiltonian

$$H_{\text{eff}} \approx g_{\text{eff}}(a_1^\dagger + a_2^\dagger)(a_1 - a_2)\sigma_{\text{eff}}^+ + h_{\text{eff}}(a_1 - a_2)(a_1^\dagger - a_2^\dagger)|0\rangle\langle 0| + h.c., \quad (8)$$

with the effective couplings $g_{\text{eff}} = \frac{g^2 \mathcal{A}_r \mathcal{A}_b}{\delta}$ and $h_{\text{eff}} = \frac{g^2 \mathcal{A}_r^2}{\delta}$, and $\sigma_{\text{eff}}^+ \equiv |2\rangle\langle 0|$ the raising operator in the effective two level ancilla system. If we furthermore assume the decay rate κ from $|2\rangle$ to $|0\rangle$ to be very large, i.e. $\kappa \gg g_{\text{eff}}$, the ancilla can be treated as a Markovian bath and the Born-Markov approximation can be applied to the first term $\propto g_{\text{eff}}$ [?] to obtain the effective jump operators d_1 from the main text, with a decay rate $\Lambda = \frac{g_{\text{eff}}^2}{\kappa}$. The protocol of continuous monitoring now consists of detecting the photons from spontaneous emission of the transition $|2\rangle$ to $|0\rangle$ in the ancilla system.

The second term in (9), scaling as h_{eff} , is the ac Stark shift and produces a level shift together with an effective hopping between the cavities. By choosing $A_b \gg A_r$, we can keep g_{eff} (leading to the jumps) constant, while having only a small contribution from the ac Stark shift h_{eff} . Additionally, this spurious hopping can be canceled further by introducing an extra hopping barrier in (1), i.e. $H_0 \rightarrow H_0 + J(a_1^\dagger a_2 + a_2^\dagger a_1)$ with matching $J = h_{\text{eff}}$, as can be engineered in circuit QED [?].

This protocol can be extended straightforwardly to a whole chain of cavities, by coupling them 2-by-2 to ancilla three-level systems. The full system is then irradiated with the two-tone drive from (3), where the \mathcal{A}_r is of staggering order and \mathcal{A}_b is uniform throughout the lattice. We this, the set of dissipators $(-1)^{j+1}d_j$ (1) from the main text will be found, with an irrelevant phase factor ± 1 . Registering a photon click in the ancilla connecting site j and $j+1$ then amounts to the detection of the jump d_j in the cavity chain. In Fig. 1(b) we provide an overview of the energy scales introduced in this derivation to obtain the effective jump operator d_1 .

B. Controlled dephasing

While dephasing is an omnipresent type of dissipation in many physical systems, for the purposes of this work, we want to engineer it in a controllable way throughout the chain to register the jumps $c_j = a_j^\dagger a_j$. Similar to (8) for phase locking, here we need to engineer an effective coupling between each cavity and a new ancilla two-level system of the form

$$H_{\text{eff}} = g_{\text{eff}} a^\dagger a \sigma_{\text{eff}}^x. \quad (9)$$

In the strongly dispersive regime for the ancilla, where the Born-Markov approximation holds, the recording of a spontaneous spin decay event in the ancilla then corresponds to a dephasing jump $a^\dagger a$ in the cavity.

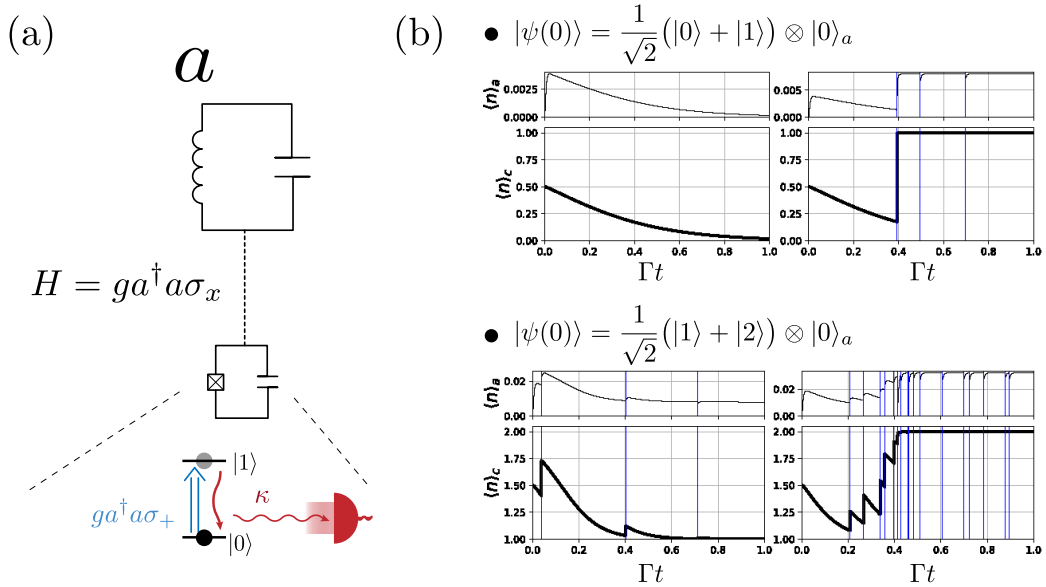


Figure 2. (a) Schematic of a cavity coupled to an ancilla qubit with coupling $H \sim a^\dagger a\sigma_x$ to record the dephasing jumps as ancilla decay jumps. (b) Lower panels show cavity occupation $\langle n \rangle_c$ starting from two different initial states that are a superposition of two number states, with the ancilla in state $|0\rangle$. Upper panels show the ancilla qubit occupation $\langle n \rangle_a$. Blue vertical lines are ancilla decay jumps. For each case, two trajectories are plotted that converge to lower number state (left panels) or the higher number state (right panel) of the initial superposition. The first case (left) shows few decay jumps, while the second (right) shows many jumps.

The same idea as for the phase-locking protocol could be followed, where each cavity is coupled to a strongly anharmonic three-level ancilla with a coupling of the form $V \sim (a + a^\dagger)(\Sigma_j + \Sigma_j^\dagger)(\Omega(t) + \Omega^*(t))$ and a drive $\Omega(t) = \mathcal{A}_r e^{i\omega_r t} + \mathcal{A}_b e^{i\omega_b t}$ that has the same relationship for the frequencies as (3). The same analysis would then result in a coupling of the form $\sim a^\dagger a\sigma_{\text{eff}}^x$ for each cavity, leading to the dephasing jump operators of the form $c \sim a^\dagger a$ in the Born-Markov approximation and jumps that can be registered again as spontaneous emission events in the ancilla. The ac Stark shift would then simply correspond to a small (uniform) level shift of the cavity modes from H_0 (1).

C. Simulation of the monitoring scheme

We start with providing a simulation of the scheme for dephasing, for which a cavity is coupled to an ancilla qubit with a coupling $H = ga^\dagger a\sigma_x$, as illustrated in 2(a). The ancilla has a large decay rate $\kappa = 500g^2/\Gamma$, with Γ the effective dephasing rate. In Fig 2(b) we show trajectories for an initial state that is a product state of a superposition of two number states for the cavity and the ground state for the ancilla, i.e. $|\psi(0)\rangle = \frac{1}{\sqrt{2}}(|n_1\rangle + |n_2\rangle) \otimes |0\rangle_a$, with $n_1 < n_2$. The stochastic evolution for the cavity number $\langle n \rangle_c$ (lower panels) and ancilla number $\langle n \rangle_a$ (upper panels) are shown and the ancilla decay jumps are indicated with blue vertical lines. Dephasing jumps $a^\dagger a$ favor higher number states, while the anti-Hermitian $H = -\Gamma/2a^\dagger a$ decreases the norm of these, bringing the cavity to lower number states, so that the overall probability to end in state $|n_1\rangle$ or $|n_2\rangle$ for the initial state is 1/2.

When monitoring the ancilla decay jumps, we see this as well; many jumps (blue vertical lines) in the ancilla lead to $|n_2\rangle$, while few jumps (and therefore anti-Hermitian evolution dominates) lead to $|n_1\rangle$. If we start from a superposition of $|0\rangle$ and $|1\rangle$, only one jump is needed to bring you to $|1\rangle$, as we also see in the picture after a single ancilla decay (upper right). We thus conclude that dephasing jumps on the cavity can be inferred by monitoring the spontaneous emission events of the ancilla qubit. Note also that $\langle n \rangle_a \approx 0$ at all times (upper panels) due to the large ancilla decay rate, which allows us to make the Born-Markov approximation to effectively obtain the dephasing jumps.

We would like to stress here once more that the standard monitoring scheme from quantum non-demolition (QND) measurements relies on a coupling of the form $H \sim a^\dagger a\sigma_z$, which is inherently different from our proposal. In the QND case, the evolution of the cavity number can be inferred by measuring the qubit resonance repeatedly in time, since the number of particles in the cavity results in a level shift for the qubit. In the same spirit, the parity of a cavity was monitored by performing qubit measurements at a high repetition rate after applying a controlled phase gate [?]. However, in this work the cavity state is always projected upon a parity subspace, such that cavity losses

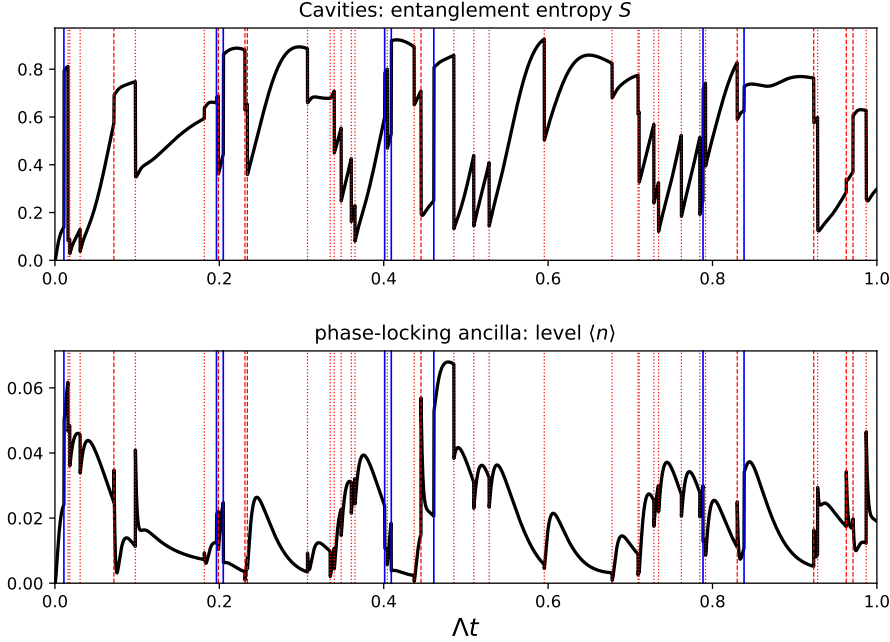


Figure 3. An example of a trajectory for two cavities coupled to the phase-locking ancilla with local dephasing. The upper panel shows the entanglement entropy S of one cavity with the other, while the lower panel shows the ancilla expectation $\langle n \rangle$. Decay jumps in the phase-locking ancilla are indicated with blue lines, while red lines correspond to dephasing jumps in the cavities.

can be inferred, whereas our primary interest lies in tracking the occurrence of the same quantum jumps that we engineer with the ancilla coupling, *without* performing a (partially) projective measurement.

In Fig. 3 we show a simulation of the setup depicted in Fig. 3b of the main article. We consider two cavities that are coupled to an ancilla qubit with H_{eff} (8), where we neglect ac Stark shift ($g_{\text{eff}} \gg h_{\text{eff}}$). The ancilla qubit is very lossy, with a decay rate $\kappa = 500g_{\text{eff}}^2/\Lambda$. In addition, each cavity is subject to local dephasing $c_j = a_j^\dagger a_j$ with a rate $\Gamma = 10\Lambda$.

The upper panel from Fig. 3 shows the Von Neumann entropy of the first cavity S , quantifying its amount of entanglement with the second (or the other way around), while the lower panel shows the ancilla qubit occupation $\langle n \rangle$. Since the decay of the qubit κ is very large, it is almost always found in the ground state $|0\rangle$. When an ancilla decay jump is detected (blue lines) we see an abrupt rise in S (upper panel) and, of course, a sudden drop of the ancilla to $|0\rangle$ – this corresponds to applying the phase-locking jump d_j to the cavities in the Born-Markov approximation [?]. On the other hand, if a dephasing jump (red lines) is recorded in cavity 1 (dotted) or cavity 2 (dashed) we (almost always) see an abrupt drop of S and a rise of ancilla $\langle n \rangle$. Therefore, this illustrates once more that dephasing and phase-locking are incompatible and that a phase-locking jump might evoke a dephasing jump and vice versa, resulting often in a series of jumps within a short time, as can be seen in the trajectory around $\Delta t \approx [0.2, 0.4, 0.8]$. Also interesting, when no jump is detected over a period of time, we still see continuous dynamics in both S and $\langle n \rangle$, as would be found from the evolution with the anti-Hermitian cavity Hamiltonian from the quantum jump approach. As a consequence, both the detection *and* the absence of a quantum jump yield information about the quantum state for an observer that tracks the dynamics of the system with a continuous monitoring scheme. In conclusion, the detection of a decay jump in the ancilla coupled to the two cavities corresponds to the recording of a phase-locking jump d_j .

II. THE GUTZWILLER MASTER EQUATION

For the Gutzwiller approach we start from the reduced density matrix of a trajectory state $|\psi\rangle$, defined as $\rho_j[|\psi\rangle] = \text{tr}_j(|\psi\rangle\langle\psi|)$, where $\text{tr}_j \cdot$ means tracing over all sites other than j . After averaging over trajectory states $|\psi\rangle$, we find

an effective master equation for the averaged ρ_j only, which is of the form

$$\partial_t \rho_j = \text{tr}_{\bar{j}} \{ \partial_t \rho \} = \text{tr}_{\bar{j}} \{ \mathcal{L}(\rho) \}, \quad (10)$$

where ρ is the full system density matrix and $\mathcal{L}(\rho)$ the full Liouvillian of the system,

$$\mathcal{L}(\rho) = \sum_i \gamma_i \left(c_i \rho c_i^\dagger - \frac{1}{2} (c_i^\dagger c_i \rho + \rho c_i^\dagger c_i) \right), \quad (11)$$

with c_i the jump operators and γ_i the corresponding dissipation rates rates.

While it is easy to check that the master equation is invariant under a transformation to new jump operators \tilde{c}_i of the form $\tilde{c}_i \equiv \sum_j U_{ij} c_j$ with U some unitary matrix, we emphasize that the validity of the Gutzwiller approach to the master equation is intimately related to the unraveling associated with our monitoring scheme, with the *local* jumps (1) and (2) from the main text. In other words, it is exactly this what motivates us to interpret ρ_j as the averaged on-site reduced density matrix from the trajectories arising in our unraveling.

A. Phase locking

The phase-locking jumps d_j act only on sites j and $j+1$. The Gutzwiller approach now relies on the assumption that one can approximate the two-site reduced density matrix as $\rho_{j,j+1} = \rho_j \otimes \rho_{j+1}$. This leads to the effective on-site Liouvillian for the jump operator d_j of the local density matrix ρ_j

$$\tilde{\mathcal{L}}_j^{(\text{pl})}(\rho_j) = \text{tr}_{j+1} \left\{ d_j (\rho_j \otimes \rho_{j+1}) d_j^\dagger - \frac{1}{2} \left(d_j^\dagger d_j (\rho_j \otimes \rho_{j+1}) + (\rho_j \otimes \rho_{j+1}) d_j^\dagger d_j \right) \right\} \quad (12)$$

We then find a mean-field master equation for the local density matrix ρ_j (we omit the index ‘ j ’ and the factor ‘2’ comes from the two jumps d_{j-1} and d_j acting on site j)

$$\partial_t \rho_j \Big|_{\text{pl}} = 2 \tilde{\mathcal{L}}^{(\text{pl})}(\rho_j). \quad (13)$$

After working out (12), we find that

$$\tilde{\mathcal{L}}^{(\text{pl})}(\rho) = \tilde{\mathcal{L}}^{(\text{pl,d})}(\rho) + \tilde{\mathcal{L}}^{(\text{pl,e})}(\rho) + (\tilde{\mathcal{L}}^{(\text{pl,e})}(\rho))^\dagger, \quad (14)$$

with

$$\tilde{\mathcal{L}}^{(\text{pl,d})}(\rho) = n \left(a^\dagger \rho a - \frac{1}{2} \{ a a^\dagger, \rho \} \right) + (n+1) \left(a \rho a^\dagger - \frac{1}{2} \{ a^\dagger a, \rho \} \right) + a^\dagger a \rho a^\dagger a - \frac{1}{2} \{ a^\dagger a a^\dagger a, \rho \}, \quad (15)$$

where $n = \langle a^\dagger a \rangle = 1$, in our case, is the mean on-site particle number.

We furthermore find the contribution for generating non-diagonal order in ρ_j

$$\begin{aligned} \tilde{\mathcal{L}}^{(\text{pl,e})}(\rho) &= \frac{1}{2} (\langle a^\dagger a a^\dagger \rangle + \langle a^\dagger a^\dagger a \rangle) (\rho a - a \rho) - \langle a^2 \rangle \left(a^\dagger \rho a^\dagger - \frac{1}{2} \{ a^\dagger a^\dagger, \rho \} \right) \\ &\quad + \langle a \rangle \left(a^\dagger a \rho a^\dagger - \frac{1}{2} \{ a^\dagger a^\dagger a, \rho \} - a^\dagger \rho a^\dagger a + \frac{1}{2} \{ a^\dagger a a^\dagger, \rho \} \right). \end{aligned} \quad (16)$$

It is now easy to check that a coherent state $|\alpha\rangle$, having $a|\alpha\rangle = \alpha|\alpha\rangle$, is a dark state of the local master equation – it annihilates the r.h.s. of 13. We can find the norm of α from the filling factor as $|\alpha| = \sqrt{n} = 1$, while the phase is free and set by the initial state.

B. Dephasing

The dephasing is much more straightforward because it is local and acts on single sites only. For the local density matrix we then find

$$\partial_t \rho \Big|_{\text{dp}} = \mathcal{L}^{(\text{dp})}(\rho) = a^\dagger a \rho a^\dagger a - \frac{1}{2} \{ a^\dagger a a^\dagger a, \rho \} \quad (17)$$

C. Full time evolution

The full time-evolution with the correct monitoring rates of the on-site density matrix ρ is then found as

$$\partial_t \rho = 2\eta \tilde{\mathcal{L}}^{(\text{pl})}(\rho) + \gamma \tilde{\mathcal{L}}^{(\text{dp})}(\rho), \quad (18)$$

which we can numerically integrate in time with a Runge-Kutta scheme to obtain expectation values of local observables $\langle O \rangle_t = \text{tr}[\rho(t)O]$.

Alternatively, one can look at the equation of motion for local operator expectation values directly, by evaluating $\partial_t \langle O \rangle = \text{tr}[\partial_t \rho O] = \text{tr}[\mathcal{L}(\rho)O]$, which leads to Eq. (8) from the main text when using (18).